nature photonics

LETTERS

https://doi.org/10.1038/s41566-018-0199-z

Phase-matched extreme-ultraviolet frequency-comb generation

Gil Porat[1,5]*, Christoph M. Heyl[1,2,5], Stephen B. Schoun[1,5], Craig Benko[1], Nadine Dörre[3], Kristan L. Corwin[1,4] and Jun Ye[1]*

Laser-driven high-order harmonic generation[1,2] provides spatially[3] and temporally[4] coherent tabletop sources of broadband extreme-ultraviolet (XUV) light. These sources typically operate at low repetition rates, $f_{rep} \lesssim 100$ kHz, where phase-matched HHG is readily achieved[5,6]. However, many applications demand the improved counting statistics or frequency-comb precision afforded by high repetition rates, $f_{rep} > 10$ MHz. Unfortunately, at such high f_{rep}, phase matching is prevented by steady-state plasma accumulated in the generation volume[7–11], strongly limiting the XUV average power. Here, we use high-temperature gas mixtures as the generation medium to increase the gas translational velocity, thereby reducing the steady-state plasma in the laser focus. This allows phase-matched XUV emission inside a femtosecond enhancement cavity at $f_{rep} = 77$ MHz, enabling a record generated power of ~2 mW in a single harmonic order. This power scaling opens up many demanding applications, including XUV frequency-comb spectroscopy[12,13] of few-electron atoms and ions for precision tests of fundamental physical laws and constants[14–20].

The highly nonlinear high-order harmonic generation (HHG) process requires peak laser intensities around 10^{14} W cm^{-2}, which necessitates high laser pulse energies $\gtrsim 10$ μJ, and short pulse durations $\lesssim 100$ fs, as typically reached with low-repetition-rate, chirped-pulse amplified[21] laser systems. However, high repetition rates are desirable for applications such as photoelectron spectroscopy[22–25] and microscopy[26], as well as electron–ion coincidence spectroscopy[27,28], which are limited by counting detection or space-charge effects to a few XUV ionization events per shot. Most notably, precision phase stabilization required for frequency-comb spectroscopy[12,13] becomes increasingly challenging when f_{rep} becomes too small, for example, a few megahertz or lower. Recent efforts allowed HHG to be directly driven at $f_{rep} \gtrsim 1$ MHz, using either the direct output of a high-power oscillator[22,29] or the coherent combination of several fibre amplifiers[30]. Achieving the necessary intensity for HHG with $f_{rep} \gg 10$MHz requires lasers with average power in the kilowatt range. Apart from one demonstration at 20 MHz, where the measured XUV power was extremely low[31], higher repetition rates up to 250 MHz[32] have been facilitated only by using passive enhancement cavities, which store ~10 kW of laser power, where a gas jet is introduced at an intracavity focus[7,10–12,33–35].

In a macroscopic extended medium, efficient HHG requires matching the phase velocities of the generating laser and the generated fields. This can be achieved by balancing neutral and plasma dispersion, the geometric phase shift due to focusing (the Gouy phase), and the HHG intrinsic dipole phase[5,36]. Achieving this balance becomes increasingly challenging as the repetition rate increases above ~10 MHz. The reason for this difficulty is that the plasma generated by one pulse does not have time to clear the focal volume before the next laser pulse arrives and generates even more plasma. Consequently, a high-density steady-state plasma is formed[8,9], which is highly dispersive (see Fig. 1a), making phase matching unattainable. Although phase-matched HHG has been demonstrated at a repetition rate of 10.7 MHz[30], it has not been previously achieved at higher repetition rates, to the best of our knowledge.

Having identified the steady-state plasma as the main limitation for phase matching, we study its formation dynamics on the relevant timescale, which is the laser pulse repetition period $\tau_{rep} = 1/f_{rep}$. To this purpose, we define two dimensionless parameters: ξ_{ion} and ξ_{beam}, the number of laser pulses that enter the gas jet during the time it takes an ion to clear the ion-generation volume or during the transit time of an atom through the laser beam volume, respectively. The accumulation of plasma over many pulses stems directly from the intensity-dependent ξ_{ion}. However, in order to separate the highly nonlinear intensity dependence of plasma accumulation from the effects of other experimental parameters, it is more convenient to use the intensity-independent parameter ξ_{beam}.

The precise definitions of ξ_{ion} and ξ_{beam} are as follows: $\xi_{ion} = \tau_{ion}/\tau_{rep}$, where τ_{ion} is the transit time of an ion through the full-width at half-maximum (FWHM) of the intensity-dependent ion-generation volume. This volume is defined by the ionization probability profile created by a single laser pulse, $\eta_{pulse}(x)$, which is calculated numerically (see Supplementary Information). Similarly, $\xi_{beam} = \tau_{beam}/\tau_{rep}$, where $\tau_{beam} = \sigma_{FWHM}/v_{gas}$. Here, σ_{FWHM} is the full-width at half-maximum of the intensity profile and $v_{gas} = \sqrt{5RT/M_{avg}}$ is the translational velocity of the gas[37] perpendicular to the laser propagation direction, with R denoting the universal gas constant, T the gas stagnation (backing) temperature, and M_{avg} the weighted-average molar mass of the monatomic gas mixture.

The steady-state ionization fraction η_{steady} (spatially averaged over the intensity profile) is shown in Fig. 1b as a function of ξ_{beam} and laser intensity, where the contour lines correspond to ξ_{ion}. The HHG yield from a single atom increases with intensity; however, Fig. 1b shows that a higher intensity also corresponds to a higher steady-state ionization fraction. For a fixed intensity, η_{steady} increases with a higher repetition rate or slower gas jet. We note that decreasing the spot size at fixed peak intensity would also decrease the steady-state ionization; however, it would reduce the size of the generation volume, thus preventing a gain in the total harmonic yield.

[1]JILA, NIST and the University of Colorado, Boulder, CO, USA. [2]Department of Physics, Lund University, Lund, Sweden. [3]University of Vienna, Faculty of Physics, VCQ, Vienna, Austria. [4]Department of Physics, Kansas State University, Manhattan, KS, USA. [5]These authors contributed equally: Gil Porat, Christoph M. Heyl, Stephen B. Schoun. *e-mail: gilpor@gmail.com; ye@jila.colorado.edu

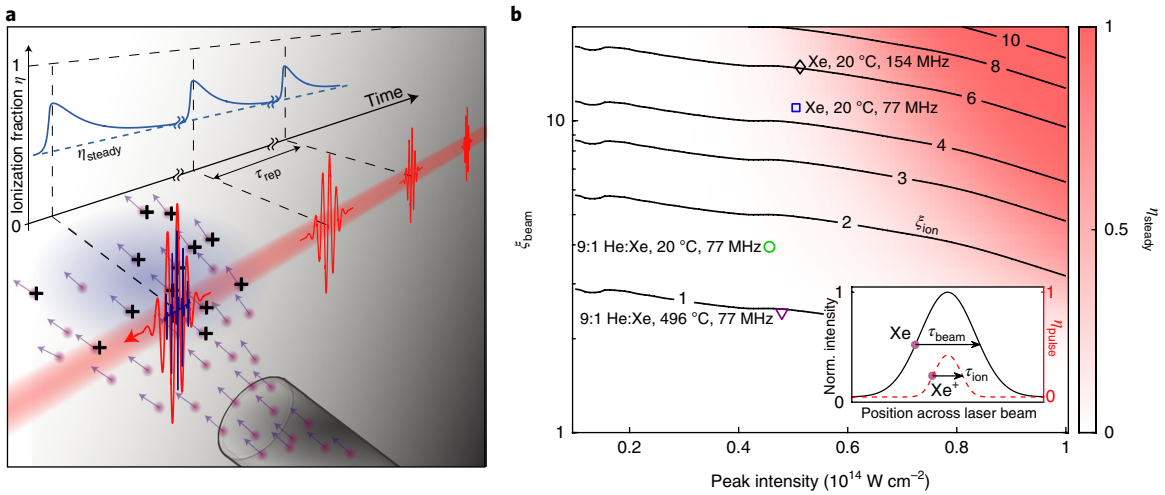

Fig. 1 | Plasma dynamics in high-repetition-rate high-harmonic generation. a, Overview. A train of femtosecond laser pulses crosses and ionizes a xenon gas jet. The interval between consecutive pulses, $\tau_{rep}=1/f_{rep}$, is smaller than the plasma transit time through the ionization volume, resulting in a high steady-state ionization fraction, η_{steady}. **b**, Spatially averaged steady-state ionization fraction, η_{steady} (colour scale), as a function of peak laser intensity and the number of laser pulses that cross the gas jet during the gas transit time through the laser beam, $\xi_{beam}=\tau_{beam}/\tau_{rep}$. The contour lines show the intensity-dependent number of laser pulses $\xi_{ion}=\tau_{ion}/\tau_{rep}$ that cross the gas jet during the time it takes an ion to clear the ion-generation volume, as illustrated in the inset. The black diamond ($\eta_{steady}=17\%$), blue square ($\eta_{steady}=11\%$), green circle ($\eta_{steady}=1.1\%$) and purple triangle ($\eta_{steady}=0.2\%$) indicate experimental conditions of optimal 11th harmonic yield for various gas and laser parameters.

The ionization fraction is linked to the phase-matching conditions, thus determining directly the XUV yield. In HHG, the phase mismatch is usually expressed as a wavevector mismatch[5,6,38]:

$$\Delta k \approx \rho\left((1-\eta)\left|\frac{\partial \Delta k_n}{\partial \rho_n}\right| - \eta\left|\frac{\partial \Delta k_p}{\partial \rho_p}\right|\right) - |\Delta k_g| \qquad (1)$$

Here, ρ, ρ_n and ρ_p are the total, neutral and plasma densities, respectively, η is the ionization fraction, Δk_n and Δk_p are the wavevector mismatches due to neutral and plasma dispersion, respectively, and Δk_g is the geometric wavevector mismatch due to the Gouy phase dispersion. Δk_g and $\partial \Delta k_{n,p}/\partial \rho_{n,p}$ are independent of $\rho_{n,p}$. We have not included the intensity-dependent dipole phase contribution to Δk, as it is negligible in our conditions where the generation medium is much shorter than the Rayleigh length of the generating beam[39]. An optimum harmonic yield is reached for $\Delta k=0$, corresponding to an infinite coherence length $L_{coh}=\pi/\Delta k$. From equation (1) we see that the neutral and plasma dispersion can compensate the Gouy phase shift for a certain gas density, but only if the ionization fraction stays below a critical value η_{crit}. As the HHG radiation is absorbed by the generation medium, the effective coherence length is limited; therefore, the maximum yield is absorption-limited. A simplified one-dimensional analysis shows that, for a given absorption length, the harmonic yield will reach at least half of its optimum when the coherence length is sufficiently long such that $L_{abs}/L_{coh}\leq 0.2$ (ref. [5]), where $L_{abs}=(\sigma\rho)^{-1}$ is the absorption length with absorption cross-section σ. Since HHG is a highly nonlinear process, phase matching is most important near the peak of the laser pulse. Figure 2a shows the spatially averaged L_{abs}/L_{coh} at the peak of the pulse, simulated for the 11th harmonic ($\lambda_{11}=97$ nm) under our experimental conditions (see Supplementary Information), on the same axes as those used to display the steady-state ionization fraction in Fig. 1b. The expected trend of improved phase matching with lower steady-state ionization, which is reached for faster gas jet velocities and lower intensities, is clearly visible.

Phase matching becomes possible when the steady-state ionization fraction drops below the critical value, $\eta_{steady}<\eta_{crit}$. This is expected to occur in the few-pulse regime, $\xi_{ion}=2$–4, where a significant part of the plasma clears the generation volume between consecutive pulses. When $\xi_{ion}=1$, we enter the single-pulse regime, where $\eta_{steady}\approx 0$, and phase matching no longer improves as ξ_{ion} approaches 0 (see Supplementary Information). In order to get into the phase-matched regime, which has not been done for previous HHG work at $f_{rep}\gg 10$MHz, we increase the gas velocity by increasing its temperature or by seeding the heavy generator gas (Xe) in a light carrier gas (He) (that is, decreasing M_{avg})[11,32,37]. Under our experimental conditions (77 MHz, focal spot size $\sigma_{FWHM}=41$ µm, $I_{peak}\approx 5\times 10^{13}$ W cm^{-2}) we expect to reach $\xi_{ion}\approx 2$ when the helium fraction is about 80%, corresponding to a gas speed of 648 m s^{-1} (compared to 305 m s^{-1} for pure Xe) at room temperature (see Figs. 1b and 2a). The ionization potential of He (24.6 eV) is much higher than that of Xe (12.13 eV), thus, at our laser intensity, helium does not contribute to XUV emission and does not add any more plasma. We note that the He dispersion is comparable to the Xe dispersion in a 9:1 He:Xe gas mix, and XUV absorption in He is negligible for harmonic orders ≤21.

We perform HHG in an enhancement cavity (see Fig. 1 in ref. [12]), where the driving laser power is enhanced by a factor of ~200 at repetition rates of 154 MHz or 77 MHz chosen via pulse picking (see Methods for details). All measurements reported in this letter were taken while sweeping the cavity length across its resonance at a rate much slower than the cavity lifetime. Locking the cavity length allows us to maintain continuous XUV operation over several minutes at ~80% of the sweep value, limited by hydrocarbon contamination of the grating outcoupler (see Supplementary Information for details). Reducing the steady-state plasma level in the HHG generation volume comes with additional benefits for intracavity HHG, since the dependence of η_{steady} on laser intensity contributes to optical bistability and coupling to higher-order transverse modes due to plasma lensing, and these mechanisms limit the intracavity focal intensity[8]. Significant intensity clamping also stems from nonlinear effects associated with the dynamics of ionization on a single-pulse timescale (for example, blue shifting[7–9,11]), which are inevitably present during HHG.

Figure 2b,c shows the experimentally generated power S_q of the harmonic order $q=11$ and 17 ($\lambda_{17}=63$ nm), as a function of

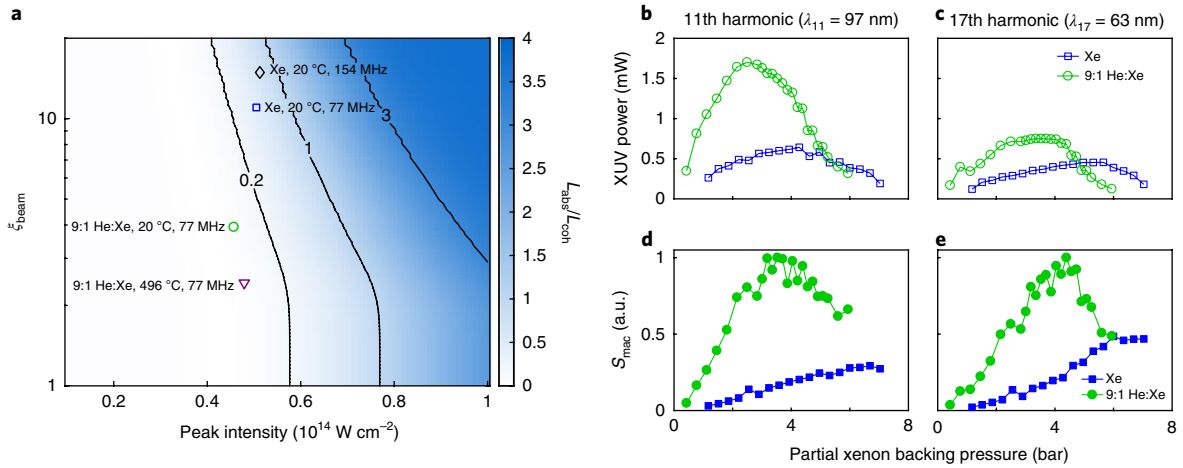

Fig. 2 | Phase-matching high-repetition-rate high-harmonic generation. a, Phase-matching figure-of-merit, spatially averaged over the beam profile, at the peak of the laser pulse, L_{abs}/L_{coh} (colour scale and contour lines), for the 11th harmonic, as a function of peak laser intensity and ξ_{beam}. Phase matching requires $L_{abs}/L_{coh} \lesssim 0.2$ (ref. [5]). The markers correspond to the same experimental conditions as displayed in Fig. 1b. **b**,**c**, Measured 11th and 17th harmonic power versus partial xenon backing pressure. **d**,**e**, The macroscopic response S_{mac}, which is the measured harmonic power divided by the measured single-atom response. The overturning peaks in the 9:1 He:Xe gas mix curves in **d** and **e** indicate phase matching.

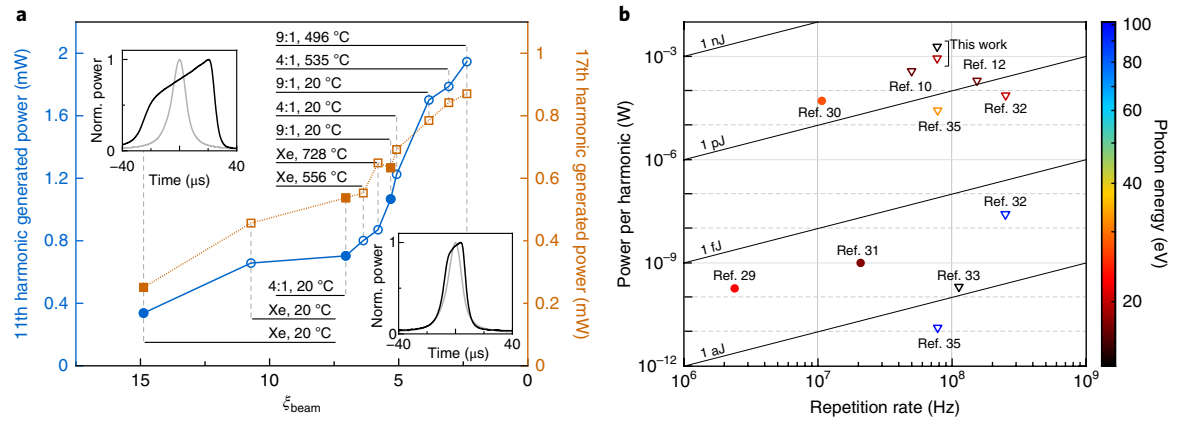

Fig. 3 | Power scaling of high-repetition-rate high-harmonic generation. a, Experimentally generated 11th and 17th harmonic power as a function of ξ_{beam} for experimental conditions with different repetition rates (filled and open markers correspond to 154 and 77 MHz, respectively), He:Xe gas mixes, and gas temperatures. Each point corresponds to the peak of a pressure-curve analogous to Fig. 2b,c. The insets show the intracavity laser power while sweeping over the cavity resonance with gas (black) and without gas (grey) for the smallest and largest ξ_{beam}. **b**, Overview of experimentally generated power per harmonic above 10 eV at repetition rates above 1 MHz, in the single-pass configuration (circles)[29–31] and the intracavity configuration (triangles)[10,12,32,33,35]. The photon energy is indicated by the marker colour. For the cases where the cavity out-coupling efficiency was not reported, we assume 10% and 5% for the Brewster plate out-coupler[10] and the hole mirror[32], respectively.

partial xenon backing pressure, for the case of a pure xenon jet and a 9:1 He:Xe gas mixture. Increasing the gas density exacerbates the aforementioned detrimental effects of the plasma in the enhancement cavity[7–9,11], leading to a decreased intracavity intensity I as the backing pressure is increased. In order to remove the ambiguity between the effects of phase matching and intracavity intensity on harmonic yield, we measured the nonlinear intensity-dependence of the single-atom response I^{N_q} for each of the two harmonics (see Supplementary Information for details). In Fig. 2d,e we plot the harmonic power divided by the single atom response, $S_{q,\mathrm{mac}} = S_q / I^{N_q}$; thus we remove the effect of the variation in generating intensity. For each of the two harmonics, we observe a clear peak for the case of the gas mix, as expected for phase-matched and absorption-limited generation (see equation (1)) (other mechanisms are ruled out; see Supplementary Information), while for pure xenon we obtain a saturation behaviour with no discernible peak. The saturation occurs since increasing the pressure causes the intensity, and correspondingly the ionization fraction, to decrease. The drop in ionization fraction balances the increase in the density as the harmonic power approaches zero due to the decreasing intensity. These results indicate that phase matching is reached when the gas mix is used.

We experimentally studied the dependence of generated harmonic power on ξ_{beam} using different gas mixes and temperatures, as displayed in Fig. 3a. Both the 11th and 17th harmonic powers monotonically increase as ξ_{beam} decreases. For both harmonics, the power increases with a roughly constant slope as ξ_{beam} is reduced to ~6. This trend stems from the increased number of neutral xenon atoms available for HHG and a slight improvement of phase matching. Beyond this point, the slope increases sharply. We attribute this increase to the onset of significant phase matching (see Supplementary Information). Indeed, as seen in Fig. 1b, $\xi_{beam} \approx 6$ corresponds to $\xi_{ion} \approx 2$ (for our intensity). As explained above, the

continued gradual reduction of the steady-state plasma is the reason the measured harmonic yield does not saturate. Our model predicts that our highest yield is ~98% of the saturated yield of the single-pulse limit (see Supplementary Information for details). Another indication that the steady-state plasma is decreasing is the mitigation of plasma-induced cavity bistability[7–9] for lower ξ_{beam}, indicated by the narrower and nearly Lorentzian intracavity power curve measured by sweeping the cavity length, shown in the insets of Fig. 3a. To connect the experimental results of Fig. 3a with our calculation of steady-state ionization and phase matching, we placed markers on Figs. 1b and 2a, which correspond to pressure-optimized 11th-harmonic conditions for various f_{rep}, ν_{gas} and σ_{FWHM}. Figure 1b shows that in the cases of a pure xenon generation medium and either a 154 MHz or a 77 MHz repetition rate, the phase-matched regime is not reached (that is, $\xi_{ion} > 4$), as opposed to a 9:1 He:Xe gas mix at a 77 MHz repetition rate at room temperature and heated (where $\xi_{ion} < 2$). Correspondingly, Fig. 2a predicts a significant improvement in phase matching for the 11th harmonic for the last two cases, as corroborated by the experimental results in Figs. 2d and 3a. Finally, we point out the fact that for the highest gas speeds, we have achieved record power levels of ~2 mW and ~0.9 mW for the 11th and 17th harmonics, respectively (see Fig. 3b). These correspond to intracavity conversion efficiencies of 1.8×10^{-7} and 8.5×10^{-8}, which are comparable to those obtained[30] with single-pass phase-matched HHG using a similar generating wavelength at $f_{rep} = 10.7$ MHz.

In conclusion, we have demonstrated phase-matched high-repetition-rate (≫10 MHz) HHG for the first time, achieving beyond milliwatt power levels per harmonic order, bringing the generated XUV brightness to a similar level as obtained from synchrotron sources[8]. Our results not only set a new power record for HHG-based XUV sources in general (including low-repetition rate systems), they also open the door to direct frequency-comb spectroscopy in few-electron systems such as He (ref. [15]) and highly charged ions[40]. We have shown that steady-state plasma mitigation is possible and critical for phase-matching high-repetition-rate HHG, and that a simple model of plasma motion is sufficient to capture all of the important dynamics involved in plasma accumulation and predict the conditions required for phase matching. The universal physical insight we provide will be indispensable for phase-matching and power-scaling HHG driven by emerging laser technology with shorter pulses, higher repetition rates and higher powers.

Methods

Methods, including statements of data availability and any associated accession codes and references, are available at https://doi.org/10.1038/s41566-018-0199-z.

Received: 12 September 2017; Accepted: 22 May 2018;
Published online: 18 June 2018

References

1. McPherson, A. et al. Studies of multiphoton production of vacuum-ultraviolet radiation in the rare gases. *J. Opt. Soc. Am. B* **4**, 595–601 (1987).
2. Ferray, M. et al. Multiple-harmonic conversion of 1064 nm radiation in rare gases. *J. Phys. B* **21**, L31–L36 (1988).
3. Bartels, R. A. et al. Generation of spatially coherent light at extreme ultraviolet wavelengths. *Science* **297**, 376–378 (2002).
4. Benko, C. et al. Extreme ultraviolet radiation with coherence time greater than 1 s. *Nat. Photon.* **8**, 530–536 (2014).
5. Constant, E. et al. Optimizing high harmonic generation in absorbing gases: model and experiment. *Phys. Rev. Lett.* **82**, 1668–1671 (1999).
6. Paul, A. et al. Phase-matching techniques for coherent soft X-ray generation. *IEEE J. Quantum Electron.* **42**, 14–26 (2006).
7. Yost, D. C. et al. Power optimization of XUV frequency combs for spectroscopy applications [Invited]. *Opt. Express* **19**, 23483–23493 (2011).
8. Allison, T. K., Cingöz, A., Yost, D. C. & Ye, J. Extreme nonlinear optics in a femtosecond enhancement cavity. *Phys. Rev. Lett.* **107**, 183903 (2011).
9. Carlson, D. R., Lee, J., Mongelli, J., Wright, E. M. & Jones, R. J. Intracavity ionization and pulse formation in femtosecond enhancement cavities. *Opt. Lett.* **36**, 2991–2993 (2011).
10. Lee, J., Carlson, D. R. & Jones, R. J. Optimizing intracavity high harmonic generation for XUV fs frequency combs. *Opt. Express* **19**, 23315–23326 (2011).
11. Mills, A. K., Hammond, T. J., Lam, M. H. C. & Jones, D. J. XUV frequency combs via femtosecond enhancement cavities. *J. Phys. B* **45**, 142001 (2012).
12. Cingöz, A. et al. Direct frequency comb spectroscopy in the extreme ultraviolet. *Nature* **482**, 68–71 (2012).
13. Kandula, D. Z., Gohle, C., Pinkert, T. J., Ubachs, W. & Eikema, K. S. E. Extreme ultraviolet frequency comb metrology. *Phys. Rev. Lett.* **105**, 063001 (2010).
14. Drake, G. W. F. & Yan, Z.-C. High-precision spectroscopy as a test of quantum electrodynamics in light atomic systems. *Can. J. Phys.* **86**, 45–54 (2008).
15. Eyler, E. E. et al. Prospects for precision measurements of atomic helium using direct frequency comb spectroscopy. *Eur. Phys. J. D* **48**, 43–55 (2008).
16. Herrmann, M. et al. Feasibility of coherent xuv spectroscopy on the 1*S*–2*S* transition in singly ionized helium. *Phys. Rev. A.* **79**, 1–15 (2009).
17. Karshenboim, S. G. Precision physics of simple atoms: QED tests, nuclear structure and fundamental constants. *Phys. Rep.* **422**, 1–63 (2005).
18. Pálffy, A. Nuclear effects in atomic transitions. *Contemp. Phys.* **51**, 471–496 (2010).
19. Ubachs, W., Salumbides, E. J., Eikema, K. S. E., De Oliveira, N. & Nahon, L. Novel techniques in VUV high-resolution spectroscopy. *J. Electron Spectrosc. Relat. Phenom.* **196**, 159–164 (2014).
20. Vogel, M. & Quint, W. Aspects of fundamental physics in precision spectroscopy of highly charged ions in Penning traps. *Ann. Phys.* **525**, 505–513 (2013).
21. Backus, S., Durfee, C. G., Murnane, M. M. & Kapteyn, H. C. High power ultrafast lasers. *Rev. Sci. Instrum.* **69**, 1207–1223 (1998).
22. Chiang, C. T., Blättermann, A., Huth, M., Kirschner, J. & Widdra, W. High-order harmonic generation at 4 MHz as a light source for time-of-flight photoemission spectroscopy. *Appl. Phys. Lett.* **101**, 071116 (2012).
23. Frietsch, B. et al. A high-order harmonic generation apparatus for time- and angle-resolved photoelectron spectroscopy. *Rev. Sci. Instrum.* **84**, 075106 (2013).
24. Wallauer, R., Reimann, J., Armbrust, N., Güdde, J. & Höfer, U. Intervalley scattering in MoS_2 imaged by two-photon photoemission with a high-harmonic probe. *Appl. Phys. Lett.* **109**, 162102 (2016).
25. Corder, C. et al. Ultrafast extreme ultraviolet photoemission without space charge. Preprint at https://arXiv.org/abs/1801.08124v2 (2018).
26. Stockman, M. I., Kling, M. F., Kleineberg, U. & Krausz, F. Attosecond nanoplasmonic-field microscope. *Nat. Photon.* **1**, 539–544 (2007).
27. Dörner, R. et al. Cold target recoil ion momentum spectroscopy: a 'momentum microscope' to view atomic collision dynamics. *Phys. Rep.* **330**, 95–192 (2000).
28. Sabbar, M. et al. Combining attosecond XUV pulses with coincidence spectroscopy. *Rev. Sci. Instrum.* **85**, 103113 (2014).
29. Emaury, F., Diebold, A., Saraceno, C. & Keller, U. Compact extreme ultraviolet source at megahertz pulse repetition rate with a low-noise ultrafast thin-disk laser oscillator. *Optica* **2**, 980 (2015).
30. Hädrich, S. et al. Exploring new avenues in high repetition rate table-top coherent extreme ultraviolet sources. *Light Sci. Appl.* **4**, e320 (2015).
31. Vernaleken, A. et al. Single-pass high-harmonic generation at 20.8 MHz repetition rate. *Opt. Lett.* **36**, 3428–3430 (2011).
32. Carstens, H. et al. High-harmonic generation at 250 MHz with photon energies exceeding 100 eV. *Optica* **3**, 366–369 (2016).
33. Gohle, C. et al. A frequency comb in the extreme ultraviolet. *Nature* **436**, 234–237 (2005).
34. Jones, R. J., Moll, K. D., Thorpe, M. J. & Ye, J. Phase-coherent frequency combs in the vacuum ultraviolet via high-harmonic generation inside a femtosecond enhancement cavity. *Phys. Rev. Lett.* **94**, 193201 (2005).
35. Pupeza, I. et al. Compact high-repetition-rate source of coherent 100 eV radiation. *Nat. Photon.* **7**, 608–612 (2013).
36. Popmintchev, T., Chen, M.-C., Arpin, P., Murnane, M. M. & Kapteyn, H. C. The attosecond nonlinear optics of bright coherent X-ray generation. *Nat. Photon.* **4**, 822–832 (2010).
37. Miller, D. R. in *Atomic and Molecular Beam Methods* Vol. 1 (ed. Scoles, G.) Ch. 2 (Oxford Univ. Press, Oxford, 1988).
38. Heyl, C. M., Güdde, J., L'Huillier, A. & Höfer, U. High-order harmonic generation with μJ laser pulses at high repetition rates. *J. Phys. B* **45**, 074020 (2012).
39. Heyl, C. M., Arnold, C. L., Couairon, A. & L'Huillier, A. Introduction to macroscopic power scaling principles for high-order harmonic generation. *J. Phys. B* **50**, 013001 (2017).
40. Crespo López-Urrutia, J. R. Frequency metrology using highly charged ions. *J. Phys. Conf. Ser.* **723**, 012052 (2016).

Acknowledgements
This work was supported by the Air Force Office of Scientific Research grant FA9550-15-1-0111, National Institute of Standards and Technology and the National Science Foundation Physics Frontier Center at JILA (PHY-1734006). C.M.H. was supported by the Swedish Research Council. K.L.C. acknowledges the support of the JILA Visiting Fellows Program.

Author contributions
All authors contributed to the design, planning and execution of the experiment. G.P., C.M.H., S.B.S., C.B. and J.Y. analysed the data. All authors contributed to the writing of the manuscript.

Competing interests
The authors declare no competing interests.

Additional information
Supplementary information is available for this paper at https://doi.org/10.1038/s41566-018-0199-z.

Reprints and permissions information is available at www.nature.com/reprints.

Correspondence and requests for materials should be addressed to G.P. or J.Y.

Publisher's note: Springer Nature remains neutral with regard to jurisdictional claims in published maps and institutional affiliations.

Methods

The main experimental system is described in detail elsewhere[4,12]; here we provide a brief overview. The laser is a Yb:fibre-amplified frequency comb delivering 120 fs pulses, spectrally centred at 1,070 nm (ref. [41]). By optionally inserting an electro-optic pulse picker before the final fibre amplifier stage, we operate with an amplifier-saturated output power of 80 W at either $f_{rep} = 154$ MHz or 77 MHz. The 3.9 m roundtrip ring cavity (single-pulse resonant for 77 MHz; two-pulse resonant for 154 MHz) is found to give the same HHG performance at 154 MHz as a 1.94 m roundtrip cavity (single-pulse resonant for 154 MHz) with the same finesse and focal spot size. In order to maintain the same peak intensity at the same average power for both repetition rates, the cavity is operated with a focal spot size of $\sigma_{FWHM} = 29$ µm at $f_{rep} = 154$ MHz, and this is increased by $\sqrt{2}$ to $\sigma_{FWHM} = 41$ µm at $f_{rep} = 77$ MHz. The focal spot size is determined experimentally from the frequency spacing of cavity-swept high-order modes. The gas jet is injected into the cavity focus with a home-made fused silica nozzle with a 36 mm temperature-controlled section wrapped in resistive heater wire, followed by a 50-µm-diameter orifice at the tip (see Supplementary Information). Differential gas pumping is maintained by a 1.5-mm-diameter orifice gas-catch assembly placed at a distance of ~0.5 mm from the nozzle orifice.

The generated XUV harmonics are outcoupled from the cavity by a flat mirror with a nano-etched surface[42] which acts as a grating for the XUV with an outcoupling efficiency of 7% and 11% for the 11th and 17th harmonics, respectively, calculated from the groove depth and period measured with an atomic force microscope. The two selected harmonics are each directed to their detectors via one grazing-incidence reflection on bare-gold mirrors. The 11th harmonic is measured with a National Institute of Standards and Technology (NIST)-calibrated Al_2O_3 windowless photoemissive detector, and the 17th harmonic is measured using an aluminium-foil-coated silicon photodiode (Opto Diode AXUV100Al). The Si photodiode is calibrated against the NIST photoemissive detector by measuring the 17th harmonic power with both detectors sequentially, under easily repeatable conditions (unheated pure Xe). We estimate the upper bound of the uncertainty in the generated harmonic power measurement to be ±7%.

Data availability. The data that support the plots within this paper and other findings of this study are available from the corresponding authors upon reasonable request.

References

41. Ruehl, A., Marcinkevicius, A., Fermann, M. E. & Hartl, I. 80 W, 120 fs Yb-fiber frequency comb. *Opt. Lett.* **35**, 3015–3017 (2010).
42. Yost, D. C., Schibli, T. R. & Ye, J. Efficient output coupling of intracavity high-harmonic generation. *Opt. Lett.* **33**, 1099–1101 (2008).